

MIT Open Access Articles

*Combinatorial discovery of polymers
resistant to bacterial attachment*

The MIT Faculty has made this article openly available. **Please share**
how this access benefits you. Your story matters.

Citation: Hook, Andrew L, Chien-Yi Chang, Jing Yang, Jeni Luckett, Alan Cockayne, Steve Atkinson, Ying Mei, et al. "Combinatorial Discovery of Polymers Resistant to Bacterial Attachment." *Nature Biotechnology* 30, no. 9 (August 12, 2012): 868–875.

As Published: <http://dx.doi.org/10.1038/nbt.2316>

Publisher: Nature Publishing Group

Persistent URL: <http://hdl.handle.net/1721.1/91141>

Version: Author's final manuscript: final author's manuscript post peer review, without publisher's formatting or copy editing

Terms of Use: Article is made available in accordance with the publisher's policy and may be subject to US copyright law. Please refer to the publisher's site for terms of use.



Published in final edited form as:

Nat Biotechnol. 2012 September ; 30(9): 868–875. doi:10.1038/nbt.2316.

Combinatorial discovery of polymers resistant to bacterial attachment

Andrew L Hook^{#1}, Chien-Yi Chang^{#2}, Jing Yang^{#1}, Jeni Luckett², Alan Cockayne², Steve Atkinson², Ying Mei^{3,8}, Roger Bayston⁴, Derek J Irvine⁵, Robert Langer^{3,6,7}, Daniel G Anderson^{3,6,7}, Paul Williams^{2,10}, Martyn C Davies^{1,10}, and Morgan R Alexander^{1,10}

¹Laboratory of Biophysics and Surface Analysis, University of Nottingham, Nottingham, UK.

²School of Molecular Medical Sciences, University of Nottingham, Nottingham, UK.

³Department of Chemical Engineering, Massachusetts Institute of Technology, Cambridge, Massachusetts, USA.

⁴School of Clinical Sciences, Queen's Medical Centre, University of Nottingham, Nottingham, UK.

⁵School of Chemistry, University of Nottingham, Nottingham, UK.

⁶David H. Koch Institute for Integrative Cancer Research, Massachusetts Institute of Technology, Cambridge, Massachusetts, USA.

⁷Harvard-MIT Division of Health Science Technology, Massachusetts Institute of Technology, Cambridge, Massachusetts, USA.

[#] These authors contributed equally to this work.

Abstract

Bacterial attachment and subsequent biofilm formation pose key challenges to the optimal performance of medical devices. In this study, we determined the attachment of selected bacterial species to hundreds of polymeric materials in a high-throughput microarray format. Using this method, we identified a group of structurally related materials comprising ester and cyclic hydrocarbon moieties that substantially reduced the attachment of pathogenic bacteria (*Pseudomonas aeruginosa*, *Staphylococcus aureus* and *Escherichia coli*). Coating silicone with these 'hit' materials achieved up to a 30-fold (96.7%) reduction in the surface area covered by bacteria compared with a commercial silver hydrogel coating *in vitro*, and the same material coatings were effective at reducing bacterial attachment *in vivo* in a mouse implant infection model. These polymers represent a class of materials that reduce the attachment of bacteria that could not have been predicted to have this property from the current understanding of bacteria-surface interactions.

© 2012 Nature America, Inc. All rights reserved.

Correspondence should be directed to M.R.A. (morgan.alexander@nottingham.ac.uk).

⁸Present address: Clemson-MUSC Bioengineering program, Clemson University, Charleston, South Carolina, USA.

¹⁰These authors jointly directed this work.

AUTHOR CONTRIBUTIONS M.R.A., M.C.D., P.W., R.L. and D.G.A. conceived the high-throughput strategy. Y.M., A.L.H. and J.Y. prepared the microarrays. J.Y. coated catheters with hit polymers. J.Y. and A.L.H. performed the HT-SC. C.-Y.C. performed the biological assays with support from S.A. D.J.I. prepared polymer for *in vivo* assays. J.L. and A.C. performed the *in vivo* assays. A.L.H., C.-Y.C., J.Y., M.R.A., M.C.D., P.W., R.B., D.G.A. and R.L. contributed to the analysis of data and the writing of the manuscript.

Note: Supplementary information is available in the online version of the paper.

COMPETING FINANCIAL INTERESTS The authors declare no competing financial interests.

Healthcare-associated infection is widely acknowledged as the most frequent adverse event in hospitals. It has been estimated that 80% of the infections acquired in hospitals involve biofilms¹. Biofilms are surface-associated bacterial communities within which bacteria have up to 1,000 times higher resistance to antimicrobials and host defenses compared with their planktonic counterparts^{2,3}. Biofilms present on the surface of medical devices provide the bacterial inocula for disease and can also serve as reservoirs of plasmids carrying antibiotic-resistance genes^{4,5}. Most strategies for reducing biofilm-associated infections focus on the modification of existing materials that are used to manufacture in-dwelling medical devices by the incorporation of antibiotics^{6,7} or other antimicrobials, such as silver salts, nitrofurazone, chlorhexidine, polymerized quaternary ammonium surfactants, antibacterial peptides and anionic nanoporous hydrogels^{8–15}. These approaches aim to kill bacterial cells that attach to a material, but we believe that greater efficacy in preventing biofilm formation might be achieved by the development of new materials that are inherently resistant to biofilm formation¹⁶. Previous attempts to use an anti-attachment strategy include poly(ethylene glycol) brushes¹⁷ and zwitterionic polymers^{18,19}. An important problem that has restricted the development of materials resistant to bacterial attachment and growth is the poor understanding of the interactions that bacteria make with surfaces, which is required for *ab initio* materials design.

To overcome this constraint, we have developed a high-throughput approach to study bacterial attachment to hundreds of materials in a parallel assay format that utilizes polymer microarrays^{20,21}. A micro-array format has previously proven useful for identifying polymeric materials that support stem cell attachment and proliferation^{22–25}. In this study polymer microarrays were adapted for the combinatorial development of materials resistant to bacterial attachment and growth (Fig. 1). *In vitro* testing has allowed us to identify a novel class of structurally related polymers that are resistant to bacterial attachment, outperforming commercially available silver-containing coatings. *In vivo* testing of the most promising of our materials has demonstrated the potential of these materials as coatings to reduce device-centered infection.

RESULTS

A library of 22 acrylate monomers was selected from those available commercially to provide wide chemical diversity, including ethylene glycol chains of various lengths, fluoro-substituted alkanes, linear and cyclic aliphatic, aromatic and amine moieties. To generate a large combinatorial space, we mixed each of 16 monomers (Fig. 1a, 1–16) as the major component with each of another 6 monomers (Fig. 1a, A–F) at ratios of 100:0 (homopolymer, 6 repeats), 90:10, 85:15, 80:20, 75:25 and 70:30 to create 576 monomer solutions. The combined monomer solutions were printed in triplicate as 300- μ m diameter spots with a height of ~20 μ m onto a poly (hydroxyl ethylmethacrylate) (pHEMA)-coated microscope slide where they were photopolymerized by a free radical mechanism to form the first-generation combinatorial polymer microarray (Fig. 1b). Hits from this first-generation polymer microarray were used to formulate the second-generation array and so on.

Bacterial microarray screening

The pathogens *P. aeruginosa*, *S. aureus* and uropathogenic *E. coli* (UPEC)²⁶ were transformed with plasmids expressing GFP to facilitate a high-throughput screen with a fluorescence intensity readout (Fig. 2a). These species were chosen as representatives of both Gram-positive (*S. aureus*) and Gram-negative (*P. aeruginosa* and UPEC) pathogens that are frequently found in medical device-associated infections^{27,28}. The polymer microarrays were incubated with a suspension of planktonic bacteria for each of the pathogens separately for 3 d (72 h) and revealed a wide range of resistance to bacterial attachment (Fig. 2b–d). To

simulate *in vivo* conditions, such as those encountered in the urinary tract, we conditioned one microarray with artificial urine for 72 h before incubation with UPEC and, in another experiment, we replaced the RPMI-1640 medium with artificial urine for a 72-h incubation with UPEC (Fig. 2e,f). Biomineralization was observed on some polymers as opaque deposits after conditioning in artificial urine and after culture in artificial urine in the absence of buffering (Supplementary Fig. 1), which stimulated greater bacterial attachment in all cases. The time period chosen provided a sufficiently stringent assay for the identification of a set of ‘hit’ materials that were resistant to bacterial attachment (Supplementary Fig. 2). The fluorescence signal (F) (Online Methods, equation (1)) was used to quantify the amount of bacterial attachment for each bacterial strain. A linear correlation ($R^2 = 0.93$) between F and surface coverage (by area), as determined by confocal measurements of biofilm after incubation with UPEC, confirmed the utility of F as a reliable estimate of bacterial attachment (Supplementary Fig. 3). In cases where polymers were formed from monomers that had opposing influences on bacterial attachment, a linear correlation between systematic variations in material composition and F was observed (Supplementary Fig. 4). For some polymers the biological behavior of the copolymer was superior to that of the homopolymers of the two constituent monomers. In one such example, the F of *P. aeruginosa* (F_{PA}) on the copolymer 13:E (85:15) was $1.0 \times 10^6 \pm 0.2 \times 10^6$ arbitrary units (AU), which was lower than the F_{PA} from the homopolymer of monomer 13 ($2.1 \times 10^6 \pm 0.2 \times 10^6$ AU) and the F_{PA} on the homopolymer of monomer E ($29.8 \times 10^6 \pm 1.1 \times 10^6$ AU) (Supplementary Fig. 5). This synergistic effect was observed for 11 of the 96 monomer pairs explored in the first-generation array and in all cases led to greater resistance to bacterial attachment, demonstrating that screening for hit materials using a copolymer library could produce copolymers with unexpected properties.

Varying levels of attachment were observed for the three bacterial species to the same polymer surfaces (Supplementary Fig. 6). This finding is unsurprising given the different surface properties and macromolecular surface composition of Gram-positive and Gram-negative bacteria²⁹ and the diverse attachment mechanisms they use, which can involve surface proteins, flagella, fimbriae³⁰ and exopolysaccharides³¹.

To assess the resistance of any given material to attachment by diverse bacterial species and exposure conditions, and as a guide to select hit monomers for further study, we developed a composite bacterial attachment parameter. The F value from each strain on each polymer composition, including UPEC incubated on artificial urine-conditioned slides and UPEC incubated in artificial urine, was normalized to the maximum F on the slide and averaged over all three replicates to produce an estimate of bacterial attachment value for all conditions and pathogens, called λ and defined in equation (2). A high value of λ indicated high bacterial attachment and therefore a poor material performance and vice versa. We plotted the value of λ in an intensity map for all first-generation polymer arrays, revealing which materials were least resistant to attachment by all three bacterial strains (red) and which were most resistant to all three (blue) (Fig. 2g). To compare the performance of each monomer used to fabricate the polymers, we determined the average λ from each of the materials containing a given monomer. The monomers were ranked by their average λ value, hence according to their resistance to bacterial attachment (Fig. 2h). Monomers 5 and B produced materials with the lowest average λ , that is, the most resistant to attachment, whereas 7 and E produced materials with the highest average λ .

High-throughput surface characterization of microarrays

To investigate the effect of polymer surface properties on bacterial attachment, we carried out high-throughput surface characterization (HT-SC) of the polymer microarray³². Techniques that probe the outermost surface of materials were used, including X-ray photoelectron spectroscopy (XPS) for quantitative elemental and functional analysis, atomic

force microscopy (AFM) for topographical characterization, time-of-flight secondary ion mass spectrometry (ToF-SIMS) for molecular characterization and water contact angle (WCA) measurement to probe the surface wettability^{20,32–34}. The influence of each property on bacterial attachment was assessed for all three bacterial strains separately. No correlation was identified between bacterial attachment and surface elemental composition (Supplementary Fig. 7), WCA or roughness (Supplementary Fig. 8), for the 496 materials studied in the first-generation array. ToF-SIMS analysis, coupled with the chemometrics technique of partial least squares (PLS) regression, has been demonstrated as a powerful technique for correlating surface chemistry represented in mass spectra with a univariate data set such as WCA^{35,36} or stem cell attachment^{24,25}. It was applied here to search for correlations between the surface chemistry of the array and the F values from each strain and to identify important surface moieties for bacterial attachment.

The PLS regression model produced by this analysis successfully predicted the F values for *P. aeruginosa* and *S. aureus* from the ToF-SIMS spectra (Fig. 3a), as evidenced by the linear relationship between the predicted and experimental F values (Fig. 3b–d), with an R^2 value of 0.68 and 0.76 for the two bacterial species, respectively. The PLS model for *S. aureus* gave a good prediction of the bacterial attachment for all polymers except those containing monomer 1, 6 or 10. No correlation was identified for UPEC ($R^2 = 0.28$). Only 17% of the materials on the array had a F_{UPEC} value >1% of $F_{\text{UPEC}_{\text{max}}}$ compared with 97% and 96% for *P. aeruginosa* and *S. aureus*, respectively. The low attachment of this strain on the materials screened made it difficult to compute a suitable PLS regression model; thus, this lack of a correlation does not exclude the possibility of a dependence of UPEC bacterial attachment on surface chemistry.

The successful prediction of attachment by *P. aeruginosa* and *S. aureus* from the ToF-SIMS spectra demonstrates that the attachment of these species is dependent on the polymer surface chemistry. More specifically, the influence of each of the hundreds of ions in the SIMS spectra on bacterial attachment is quantified by the regression coefficient, where a positive coefficient indicates that the ion in question promotes attachment, whereas a negative one indicates that the surface chemistry giving rise to the secondary ion is resistant to bacterial attachment (Fig. 3e). The surface chemical moieties assigned to secondary ion fragments with the highest PLS regression coefficients are shown in Figure 3e for both *P. aeruginosa* and *S. aureus*. In general, the presence of hydrocarbon secondary ions in spectra from materials was correlated with high resistance to bacterial attachment and oxygen-containing ions from certain pendant groups were observed to be correlated with low resistance to bacterial attachment for both *P. aeruginosa* and *S. aureus*. In particular, secondary ions consistent with cyclic carbon groups (C_4H^- , C_6H^-), ester groups (CHO_2^-), the tertiary butyl moiety (C_4H_7^+) and ions from aliphatic groups (C_2H_3^+ , C_2H_5^+ , C_3H_7^+) were correlated with lower bacterial attachment for both pathogens. Ions from ethylene glycol groups ($\text{C}_2\text{H}_3\text{O}^+$, $\text{C}_2\text{H}_3\text{O}_2^-$), and hydroxyl-containing fragments ($\text{C}_4\text{H}_5\text{O}_2^-$, $\text{C}_6\text{H}_{11}\text{O}_3^-$) correlated with higher bacterial attachment. These results point to the influence of moieties from particular monomers that are associated with the biological performance of the resultant polymer. Bacterial attachment is lower in monomers with the cyclic carbon environments as in monomers 4 and B, the relatively higher density of ester groups in materials formed from the triacrylate monomers 13 and 15, the tertiary butyl group of monomer 5 and the dimethyl hydrocarbon segment on monomers 2, 8 and 12. Bacterial attachment is greater where the ethylene glycol group is surface expressed as in polymers from monomers 1, 9, 16 and A, and where the hydroxyl group is present as in monomers 6, 7 and 10.

To determine the monomer composition most resistant to attachment by all three bacterial pathogens, we formulated a second-generation array that focused on the constituents from

the first-generation array most resistant to bacterial attachment (Fig. 1d) but with greater variation in composition for each monomer pair. Monomer 4 was included as it contained the cyclic hydrocarbon moieties identified by the ToF-SIMS ions, C_4H^- and C_6H^- , and revealed to be associated with reduced bacterial attachment by the PLS regression analysis. The top four hit monomers were selected (15, 5, 8 and B) and mixed with each other and monomer 4 at ratios of $x:(1 - x)$ where x varied from 10 to 90. This array contained 145 different materials (four replicates of each) plus four materials selected as positive controls that in the first-generation array were least resistant to bacterial attachment. Attachment after 3 d of incubation with all three bacterial pathogens, including UPEC incubated with artificial urine-conditioned slides, was assessed for the array and the λ for each material determined (Fig. 4).

Scale up from microarray spots

The six copolymer compositions (and four corresponding homopolymers) with the least bacterial attachment were chosen from the bacterial screen of the second-generation array as hit materials for further study. Scale-up from microarray spots to 8- to 10-mm diameter samples (termed coupons) was conducted to investigate the scalability of the polymers' physicochemical properties and biological performance (Supplementary Figs. 9 and 10). Initial scale-up experiments included monomer 15 (and other triacrylates), but inclusion of this monomer resulted in the formation of brittle materials that were observed to crack during the solvent extraction step. This was consistent with the formation of a highly cross-linked polymer and, thus, monomer 15 was removed from subsequent scale-up experiments. The area covered by the bacteria was at least twofold lower on all scaled-up materials compared with the positive control (monomer 7 homopolymer) (Supplementary Fig. 9a). Confocal microscopy coupled with live and/or dead staining (Supplementary Fig. 10) on the scaled-up polymer coupons revealed that, in common with the control polymer, a mixture of live and dead bacteria was attached to the materials. To simulate the more challenging *in vivo* conditioning by urine that is likely to occur on urinary catheters, *P. aeruginosa*, *S. aureus* and UPEC were incubated with polymer coupons preconditioned with artificial urine. For all three strains a greater than threefold reduction in the area of the sample covered by bacteria was observed for this assay compared with the positive control (monomer 7 homopolymer) (Supplementary Fig. 9b), suggesting that these materials are resistant to bacterial attachment in the presence of urine components. ToF-SIMS of the polymer coupons indicates that the aliphatic pendant group on monomers 4 and 8 was surface enriched compared with the equivalent microarray spots, which suggests that in some instances scaling up from a microarray spot to a coupon modifies the material surface chemistry and biological performance (Supplementary Figs. 9 and 11).

Development of medical device coatings

To establish the potential of these hit materials as effective coatings for medical devices, we dip-coated oxygen plasma activated silicone catheters with monomer solution followed by UV curing (Fig. 1e) and compared bacterial attachment with silicone catheters and a commercially available, state-of-the-art, silver-containing coating. The four homopolymers of the hit monomers, six hit copolymer formulations and polymers from monomers 6, 7 and 1:E (70:30) (positive controls) were coated along the luminal and abluminal surfaces of the catheters (Fig. 1f,g). Scanning electron microscopy (SEM) was used to verify the presence of the coatings (Supplementary Fig. 12). The coated catheters were incubated with *P. aeruginosa*, *S. aureus* or UPEC for 72 h. Representative confocal images from the coated catheters after bacterial incubation are shown in Figure 5a and the area of biofilm coverage was quantified for each species. The corresponding λ values, normalized to the biofilm area coverage as measured on silicone alone, are shown in Figure 5b.

For all three pathogens, the coated catheters had a substantially lower bacterial coverage than the silicone elastomer. Several of the hit acrylate materials were superior to the silver-hydrogel (BactiGuard)-coated latex catheter (Bardex), which has been shown to be clinically effective at reducing catheter-associated asymptomatic bacteriuria when compared with standard latex catheters²⁸. It should be noted that silver-hydrogel catheters are thought to be resistant to bacterial attachment as a consequence of the toxicity of silver ions to the bacteria, whereas our hit polymer coatings prevent attachment. The lowest area coverage for *P. aeruginosa* was achieved on the homopolymer formed from monomer 4, which had $1.2\% \pm 0.5\%$ of the surface populated with bacteria. This represents a 28-fold reduction compared with the silicone catheter, and a 17-fold reduction compared with the BactiGuard-coated Bardex catheter. For *S. aureus* the best performing copolymer was formed from monomers B:5 (70:30) and resulted in a bacterial surface area coverage of $0.5\% \pm 0.3\%$, which represents a 67-fold reduction compared to silicone and a 30-fold reduction compared to BactiGuard. For UPEC the best performing copolymer was B:4 (90:10), which resulted in $1.2\% \pm 0.6\%$ of the area populated with bacteria, representing a ninefold reduction compared to silicone and a sixfold reduction compared to BactiGuard. The homopolymer of B produced the catheter coating with the lowest λ of $2.0\% \pm 1.0\%$, and was the best material at preventing the attachment of all three different pathogens. The proportion of the surface covered for this coating was $2.3\% \pm 1.3\%$, $1.0\% \pm 0.4\%$ and $1.5\% \pm 0.7\%$ for *P. aeruginosa*, *S. aureus* and UPEC, respectively. This amounted to a 12-fold reduction in the composite parameter λ compared with an uncoated silicone catheter, and sevenfold lower than the BactiGuard-coated Bardex catheter.

There are several other different strategies that can be found in the literature to reduce bacterial attachment to surfaces that are not yet commercially available; for example, zwitterionic coatings function by preventing attachment^{18,19}. Comparison with the performance of our hits to these literature reports is difficult as experimental methodologies vary widely. Attachment of *P. aeruginosa* (PA01) after 3 h incubation on a poly(sulfobetaine methacrylate)-grafted surface has been reported to be lower by 25-fold compared to that on glass¹⁹, and in an incubation time closer to ours, a poly(carboxybetaine methacrylate)-grafted surface had 11-fold lower attachment of *P. aeruginosa* after 96-h bacterial exposure compared to glass¹⁸.

Mechanism for reduction of bacterial coverage

The absence of a correlation between bacterial attachment and the contact angle or roughness of the materials studied (Supplementary Fig. 8) suggests that the interaction of bacteria with the methacrylate or acrylate library cannot be explained simply by hydrophobic interactions or roughness only, as was previously invoked to explain bacterial performance on self-assembled monolayers, stainless steel and certain polymers³⁷. It should be noted that the bacterial cell incubation experiments were not conducted under flow conditions, thus, this assay did not assess any advantage gained from the shielding from shear that increased roughness could provide.

The ability to predict bacterial attachment from the chemistry of the materials as represented by the ToF-SIMS spectra (Fig. 3b–d) confirms that the bacteria-material interaction is dependent on surface chemistry. The PLS regression highlighted the ethylene glycol moieties and hydroxyl groups employed in these libraries for promoting the attachment of *P. aeruginosa* and *S. aureus*. The greater attachment associated with surface hydroxyl groups suggests a role for hydrogen bonding, which may be through an interaction with the lipopolysaccharides, lipoteichoic acids or exopolysaccharides present on the bacterial cell surface³¹. For materials with resistance to bacterial attachment, the PLS regression analysis identified hydrophobic moieties such as aromatic and aliphatic carbon groups when accompanied by the weakly polar ester groups. By comparison with polystyrene, a purely

hydrophobic material that is well known to support bacterial attachment (Supplementary Fig. 13)³⁸, the role of the ester group and the weakly amphiphilic structure of these hit polymers appear to be important for reduced bacterial attachment. Antibacterial behavior has previously been reported for zwitterionic materials¹⁹ where disparate chemical properties are presented in close proximity on the molecular scale analogous to the weak amphiphiles identified in this study. To further investigate the role of weakly amphiphilic acrylate materials in preventing bacterial attachment, we produced a third polymer microarray that contained homopolymers of 15 methacrylate or acrylate monomers that had aliphatic, cyclic or aromatic pendant groups. F_{PA} for *P. aeruginosa*, *S. aureus* and UPEC and λ for each material is shown in Supplementary Figure 14. The relatively high attachment of *P. aeruginosa* provided the greatest discrimination between the materials. The six materials with the lowest F_{PA} all contained cyclic or aromatic hydrocarbon groups. In contrast, the six materials with the highest F_{PA} all contained linear aliphatic carbon pendant groups, suggesting that the presence of ring structures is a determining factor for preventing bacterial attachment to methacrylate/acrylate polymers (Supplementary Fig. 14).

Confocal microscopy did not detect a significant number of either dead or live bacteria on the hit materials after 72 h incubation with planktonic bacteria (Fig. 5a), indicating that the mechanism behind the low attachment is prevention of bacterial attachment rather than a mechanism involving killing. Consistent with this conclusion, growth curves, which quantify bacterial numbers in the presence of the materials, showed no inhibition by the hit polymers for the bacterial strains used (Supplementary Fig. 15). In addition live and/or dead staining of the very low coverage of UPEC biofilm that were found revealed both live and dead cells present within the biofilm, which is typical of normal biofilms (Supplementary Fig. 10). Furthermore, there is no evidence of cytotoxicity to human cells of the polymers as the materials have been shown to support the culture of delicate embryonic stem cell lines²⁴.

The resistance of the lead acrylates discovered in this study to attachment of bacteria likely depends on the ability of bacterial cells to sense and respond to their immediate environment. This may be a consequence of the individual cells sensing the nature of the polymer surface by their cell envelope-associated sensory proteins or by specific surface structures such as flagella and pili involved in near-surface movement³⁹. It is also possible that the bacterial population collectively responds to the polymer through quorum sensing (bacterial cell-to-cell communication) mechanisms⁴⁰, such that the lack of bacterial attachment occurs through this population-dependent decision-making process. In both scenarios the mechanism may be more complex than simple physicochemical interactions between the bacteria and surface. Specific examples include the Rcs sensor kinase, which controls the expression of a number of *E. coli* genes in response to growth on a solid surface⁴¹. Furthermore, production of the *P. aeruginosa* exopolysaccharides Pel and Psl are both under quorum-sensing control⁴². Thus, it is highly likely that bacterial responses to surfaces are more sophisticated than is currently appreciated.

***In vivo* assessment of hit material**

The *in vivo* environment is more realistic than *in vitro* assessment of candidate materials with regards to eventual clinical application. We therefore carried out a subcutaneous foreign body infection model to test the efficacy of one of the hit materials (Fig. 1h). A copolymer of monomer 4 and di(ethylene glycol) methyl ether methacrylate (DEGMA) amenable to the dip-coating methodology was prepared by catalytic chain transfer polymerization (measured properties of the resultant polymer are shown in Supplementary Table 1). The DEGMA was included to tune the polymer's mechanical properties for *in vivo* use without compromising the polymer's resistance to bacterial attachment (Supplementary Figs. 16 and 17) and to exploit the ability of the oligo(ethylene glycol) moiety to reduce protein fouling⁴³ in the high protein-containing environment.

Both control silicone and dip-coated silicone catheters were implanted subcutaneously into mice and inoculated with bioluminescent *S. aureus* Xen29 by injection into the catheter lumen after 1 d. Immediately following inoculation similar bioluminescence was observed for both coated and uncoated catheters (Fig. 6). After 1 d, we observed more than a tenfold reduction in bioluminescence on the coated catheters compared with the uncoated silicone, a difference that persisted for 4 d (Fig. 6a–c). Bioluminescence requires the bacteria to be respiring aerobically, thus, it will not detect bacteria that are viable but are either dormant or growing anerobically. To investigate whether bacterial numbers on coated catheters were reduced, we euthanized the mice on day 4 and quantified the numbers of bacteria at the infection sites on the catheter and in the surrounding tissues, including kidneys and spleen. Bacterial numbers were reduced by nearly two orders of magnitude on the coated catheter compared to the uncoated catheter, and an order of magnitude reduction in bacterial numbers was observed in the tissue surrounding the implant, and in the kidneys and the spleen, suggesting a reduced amount of systemic bacteria (Fig. 6e). The reduction in bioluminescence on the coated catheter in the live animal demonstrates that the coating successfully reduced bacterial *in vivo* survival in the presence of the host defenses compared to the silicone control. We interpret the persistence of bacteria on the silicone catheter as indicative of bacteria that were able to attach to the silicone and form biofilms, thereby avoiding clearance by the host defenses. These observations suggest that the performance of the hit polymer identified *in vitro* translates to the challenging *in vivo* environment. Sufficiently small diameter (2.7 mm), silver-containing, hydrogel-coated catheters were not commercially available for the mouse model used in this study, preventing a direct comparison of the *in vivo* performance of the polymer in this animal study with the same controls as the *in vitro* experiments.

DISCUSSION

We have developed a method for the discovery of polymeric materials resistant to bacterial attachment using high-throughput surface characterization and chemometrics, which has identified simple chemical moieties that reduce bacterial adhesion to surfaces. The new class of materials discovered, which could not have been predicted from the current understanding of bacteria-material interactions, are resistant to bacterial attachment. An *in vitro* comparison after a 3-d incubation revealed up to 67-fold less bacterial attachment and biofilm formation compared with a commercial uncoated medical grade silicone, and a 30-fold lower bacterial attachment and biofilm formation than a commercial silver hydrogel coating. The resistance of one of these coatings to bacterial attachment was demonstrated *in vivo* using a mouse foreign-body infection model, which confirms the potential of the hit materials as coatings for indwelling biomedical devices. In contrast to the use of coatings that incorporate molecules that are toxic to and kill pathogens, the anti-attachment mechanism described here does not place selective evolutionary pressure on organisms to develop antimicrobial resistance.

By further developing this high-throughput screening approach to include other bacterial species (including freshly isolated clinical strains and pathogens specific to particular niches and different growth conditions), new polymeric materials may be found that are resistant to colonization by combinations of pathogens for medical devices, water purification systems, food preparation surfaces and utensils, or any other surface where bacterial adhesion is problematic.

ONLINE METHODS

Polymer array synthesis

Polymer microarrays were synthesized using methods previously described²². Monomers were purchased from Aldrich, Scientific Polymers and Polysciences, and printed onto epoxy-coated slides (Xenopore), dip-coated into 4% (w/v) pHEMA (Aldrich) using 946MP6B pins (ArrayIt) and a Pixsys 5500 robot (Cartesian) or a XYZ3200 dispensing workstation (Biodot). The arrays were dried at <50 mTorr for at least 7 d.

High-throughput surface characterization

Arrays were characterized by AFM, WCA, XPS and ToF-SIMS. ToF-SIMS measurements were conducted on an ION-ToF IV instrument operated using a monoisotopic Bi_3^+ primary ion source operated at 25 kV and in 'bunched mode'. A 1 pA primary ion beam was rastered, and both positive and negative secondary ions were collected from a $100 \times 100 \mu\text{m}$ area. Ion masses were determined using a high resolution Time-of-Flight analyzer. The typical mass resolution (at m/z 41) was just over 6,000. XPS was carried out on a Kratos Axis Ultra instrument using monochromated Al K α radiation (1486.6eV), 15 mA emission current, 10 kV anode potential and a charge-compensating electron flood. High-resolution core levels were acquired at a pass energy of 20 eV. WCA was measured using the sessile drop method on an automated Krüss DSA 100 instrument⁴⁴. A water drop with a volume of ~400 picoliter was used. AFM measurements were taken using a Nanoscope 3000A instrument in tapping mode. Silicon tips with a resonant frequency of ~300 kHz and a force constant of 40 N/m were used (Tap300Al, Budget Sensors) for dry state and silicon nitride tips with a resonant frequency of 7.5 kHz were used for fluid measurements. $5 \mu\text{m}$ regions of the polymer were taken and the root mean square (RMS) roughness was measured across this region. The ToF-SIMS spectra data were analyzed using principle component analysis (PCA), and the correlation between ToF-SIMS spectra and bacterial adhesion was analyzed using partial least-squares (PLS) regression³⁵. Both multivariate analysis methods were carried out using the Eigenvector PLS_Toolbox 3.5.

Scale-up of materials

Selected compositions were scaled up to 10-mm polymer coupons. These were prepared by casting 5 μl of monomer solution (75% (v/v) monomer, 25% (v/v) DMF and 1% (w/v) 2,2-dimethoxy-2-phenyl acetophenone) onto epoxy-functionalized slides (Xenopore) dip-coated with 4% (w/v) pHEMA in ethanol. For growth inhibition studies, 40 μl of monomer solution was pipetted into a well of a 96-well microwell plate. Samples were irradiated with UV (365 nm) for 10 min to initiate polymerization with $\text{O}_2 < 2,000$ p.p.m. The samples were dried at <50 mTorr for at least 7 d. To produce coated catheters, 4-cm long silicone lengths were cut from a silicone Foley urinary catheters (Bard, outer diameter 7.3 mm –*in vitro* or 2.7 mm –*in vivo*). The inside and outside surface was oxygen plasma treated for 5 min at 50 W. For *in vitro* use, plasma-treated catheters were immediately immersed in monomer solution for 10 s and blotted to remove excessive monomer solution before photopolymerization using UV (365 nm) for 1 min, with $\text{O}_2 < 2,000$ p.p.m. For *in vivo* studies, plasma-activated catheters were dip-coated with a 20% polymer solution in dichloromethane. The samples were then dried at <50 mTorr for at least 7 d. Polymer for *in vivo* studies was prepared by catalytic chain transfer polymerization. The resultant polymer solution was used for coating silicone catheters without further purification. Uncoated silicone catheters and BactiGuard (silver containing hydrogel)-coated latex catheters (Bardex) were used as controls. SEM imaging of coated catheters was conducted on a Jeol 6060LV variable pressure SEM. Samples were gold-coated before imaging using a Leica EM SCD005 sputter coater.

Bacterial growth conditions

Three different bacterial species, *P. aeruginosa* PAO1, *S. aureus* 8325-4 and UPEC were routinely grown on either LB (Luria-Bertani, Oxoid, UK) agar plates at 37 °C or in broth at 37 °C with 200 r.p.m. shaking. Three constitutively GFP-expressing plasmids, pGFP⁴⁵, pSB2019 and pSB2020 (ref. 46), were transformed into *P. aeruginosa* PAO1, *S. aureus* 8325-4 and UPEC, respectively, and maintained by adding appropriate antibiotics to the culture media. RPMI-1640 chemically defined medium (Sigma, UK) and artificial urine⁴⁷ were used in biofilm experiment for standardizing the conditions and mimicking CAUTI, respectively. For the *in vivo* study *S. aureus* Xen29 (Caliper) were routinely grown on Tryptic soya Broth (Oxoid, UK) at 37 °C until an OD of 0.8, washed twice in phosphate buffered saline (PBS, Oxoid, UK) and stored in aliquots of 1×10^9 c.f.u. in PBS/20% glycerol. These were then thawed and diluted with PBS before injection into the lumen of the catheter⁴⁷.

Prior to incubation with the bacteria, the microarray slides were washed in distilled H₂O for 10 min, air-dried and UV sterilized. Artificial urine-conditioned slides were incubated for 72 h at 37 °C in 15 ml of artificial urine with 5% CO₂. Subsequently, slides were washed three times in RPMI-1640 medium or artificial urine. Bacteria were grown on polymer slides under similar conditions to those previously described^{48,49}. Briefly, UV-sterilized polymer slides were incubated in 15 ml medium inoculated with diluted (OD₆₀₀ = 0.01) GFP-tagged bacteria from overnight cultures grown at 37 °C with 60 r.p.m. shaking for 24 h or 72 h. As growth medium controls, the slides were also incubated without bacteria. At the desired time points, the slides were removed and washed three times with 15 ml PBS at room temperature for 5 min. After rinsing with distilled H₂O to remove salts and air dried, the fluorescent images from the slides incubated in medium only and medium containing bacteria were acquired using a GenePix Autoloader 4200AL Scanner (Molecular Devices, US) with a 488 nm excitation laser and a blue emission filter (510–560 nm). The total fluorescence intensity from polymer spots was acquired using GenePix Pro 6 software (Molecular Devices, US). A similar bacterial assay was also applied to scaled-up coupons and 4-cm sections of coated catheters. After washing with distilled H₂O, the coupons or catheters were stained with 20 µM SYTO17 dye (Invitrogen, UK) at room temperature for 30 min. After air drying, the samples were examined using a Carl Zeiss LSM 700 Laser Scanning Microscope with ZEN 2009 imaging software (Carl Zeiss, Germany). The area covered by bacteria on the surface was analyzed using open source ImageJ 1.44 software (National Institutes of Health, US). The viability of bacteria attached to polymer surfaces was assessed by live/dead staining. Briefly bacteria were stained with 10 µM SYTO 9 green-fluorescent dye for live bacteria and 60 µM propidium iodide red-fluorescent dye for cell membrane damaged (dead) bacteria. After staining at room temperature for 30 min, the samples were rinsed with distilled H₂O, air dried and observed using Laser Scanning Confocal Microscopy. To evaluate the growth inhibitory properties of the hit polymers, polymer-coated wells were UV sterilized for 15 min and inoculated with bacteria (OD₆₀₀ = 0.01) from overnight cultures. The OD was monitored by an Infinite 200 microplate reader (Tecan, UK) at 37 °C every 30 min for 24 h to obtain the respective growth curves.

The fluorescence signal (F) from each bacterial pathogen was determined using equation (1), where F is the fluorescence intensity measured per unit area by the laser scanner after incubation with bacteria, and $F_{control}$ is the fluorescence intensity measured per unit area by the laser scanner measured on a control slide consisting of a replica array that was incubated in media for 72 h without bacteria. For polymers where F was below the limit of detection, F was made to equal 0 (Supplementary Discussion).

$$F = F_{test} - F_{control} \quad (1)$$

The bacterial performance (ι) was determined using equation (2), where the subscript to the F indicates the bacterial pathogen and the F_{max} is the maximum fluorescence signal measured on any spot on the array for a given pathogen. Artificial urine is abbreviated to 'au'. Note that ι reported for second-generation arrays and scaled-up samples did not include results of UPEC in artificial urine.

$$\iota = \frac{(F_{PA}/F_{PA_{max}} + F_{SA}/F_{SA_{max}} + F_{UPEC}/F_{UPEC_{max}} + F_{UPEC_{in\ au}}/F_{UPEC_{in\ au_{max}}} + F_{UPEC_{on\ au\ conditioned}}/F_{UPEC_{on\ au\ conditioned_{max}}})}{\div 5 \times 100} \quad (2)$$

Catalytic chain transfer polymerization

Polymer for *in vivo* studies was prepared by catalytic chain transfer polymerization: a degassed (N_2) solution of 15% (v/v) ethylene glycol dicyclopentenyl ether acrylate, 5% (v/v) di(ethylene glycol) methyl ether methacrylate (DEGMA), 0.5% (w/w) 2,2'-azobis-(2,4-dimethyl-4-methoxyvaleronitrile) and 2,000 p.p.m. tetraphenylcobaloxime boron fluoride (bis[(difluoroboryl) diphenylglyoxima to]cobalt(II)) in DCM was placed in a Schlenk flask at 35 °C for 24 h. The vessel was then placed into an ice bath for 5 min and exposed to air to terminate the polymerization. For analysis, the DCM was removed at reduced pressure at room temperature.

Polymer characterization

1H and ^{13}C nuclear magnetic resonance (NMR) spectra were acquired in deuterated chloroform on both Bruker DPX (300 MHz) and AV (400 MHz) instruments. Differential scanning calorimetry (DSC) measurements were conducted on a DSC Q2000 (TA Instruments). Samples were placed in a Tzero Hermetic Pan with a pressed lid. Heat flow was measured against a sealed empty pan. Sample was cycled between -40 °C and 90 °C 3 times at 10 °C/min. Number-average molecular weight (M_n), weight-average molecular weight (M_w), and dispersity (PD) were obtained by gel permeation chromatography (GPC) with a fitted IR detector. Polymer samples (7 mg/ml) dissolved in tetrahydrofuran were flowed (1 ml/min) through a PLgel 5 mm Guard column (Polymer Laboratories) and two PLgel 5 mm MIXED-C columns (Polymer Laboratories) at 40 °C. Fatigue testing was carried out on a Mayes Servohydraulic testing machine with a set of Instron wedge grips with vee jaws. The sample length between the two grips was 6 cm. The sample was bent 500 times and the total distance of movement between the two grips during bending was 1cm.

Murine catheter implant model

To evaluate the *in vivo* resistance of polymer materials to bacterial attachment, the real time, non-invasive catheter foreign body implant model was used⁵⁰. A 1-cm coated catheter segment was inserted subcutaneously into female BALB/c mice, 19–22 g (Charles River). The animals were allowed to recover with regular observation for 24 h before anesthesia with isoflurane and injection of 1×10^5 *S. aureus* Xen29 (Caliper Life Sciences Inc) in 50 μ l PBS into the lumen of the catheter using a 31 gauge needle and syringe. Mice were imaged for up to 5 min before (to assess background luminescence) and 10 min after initial bacterial inoculation, and then every 24 h, using an IVIS spectrum camera (Caliper). EMLA cream was applied daily after imaging and weight and clinical condition of animals recorded.

The total photon emissions from the catheter implantation site were quantified by using the living image software package (Xenogeny Corp.), over a 4-d period. At day 4 the mice were humanely killed and the catheter and surrounding tissue removed, the mouse kidneys and spleen harvested, and the number of *S. aureus* Xun 29 colony-forming units (cfu) present

determined using standard procedures⁵⁰. The cfu counts were normalized to the mass of tissue taken. Reported bioluminescence values had the background luminescence measured from uninoculated inserted catheters subtracted. In each experiment, three mice were implanted with control or coated catheters and the experiment repeated on three occasions with data from $n = 9$ for each group pooled for statistical analysis.

In pilot studies, Nano-ct, computed tomographic scans were used to confirm the subcutaneous localization of the catheter and were acquired using a Nanoect/CT (Bioscan). Briefly, after catheter insertion, mice were anesthetized using isoflurane and scanned at 45 kVP, using high-resolution parameters. The resulting images were reconstructed and analyzed using invivoscope software.

Surgical details of murine catheter implant model

All animal work was approved following local ethical review at Nottingham University and performed under Home Office license authority. Female BALB/c mice, 19–22 g (Charles River) were housed in IVCs under a 12 h light cycle, with food and water *ad libitum*. Briefly, the experimental procedure was carried out as follows. One hour before catheter implantation, analgesic (Rymadil (Pfizer) 2.5 mg/kg) was administered by subcutaneous injection. Animals were anesthetized using isoflurane, hair on one flank removed by shaving and the shaved area sterilized with hydrex clear (Ecolab). A 10-mm incision was made in the flank, a subcutaneous pocket created and 1-cm segment of catheter (TReleflex scale Fr8) inserted. The incision was then closed with Vetbond (3MM) and EMLA cream (AstraZeneca) applied to the implantation site.

Supplementary Material

Refer to Web version on PubMed Central for supplementary material.

Acknowledgments

Funding from the Wellcome Trust (grant no. 085245 and support from N. Shepherd) and the Medical Research Council UK (for the *in vivo* work; grant no. G0802525) is gratefully acknowledged. M. Alexander gratefully acknowledges the Royal Society for the provision of his Wolfson Research Merit Award. Assistance with ToF-SIMS measurements from D. Scurr is kindly acknowledged. Assistance with the preparation of polymer for *in vivo* studies by E. Eaves, N. Nguyen and J. Li is kindly acknowledged.

References

1. Davies D. Understanding biofilm resistance to antibacterial agents. *Nat. Rev. Drug Discov.* 2003; 2:114–122. [PubMed: 12563302]
2. Costerton JW, Stewart PS, Greenberg EP. Bacterial biofilms: a common cause of persistent infections. *Science.* 1999; 284:1318–1322. [PubMed: 10334980]
3. Smith AW. Biofilms and antibiotic therapy: is there a role for combating bacterial resistance by the use of novel drug delivery systems? *Adv. Drug Deliv. Rev.* 2005; 57:1539–1550. [PubMed: 15950314]
4. Danese PN. Antibiofilm approaches: prevention of catheter colonization. *Chem. Biol.* 2002; 9:873–880. [PubMed: 12204686]
5. Krol JE, et al. Increased transfer of a multidrug resistance plasmid in *Escherichia coli* biofilms at the air-liquid interface. *Appl. Environ. Microbiol.* 2011; 77:5079–5088. [PubMed: 21642400]
6. Darouiche RO, et al. A comparison of two antimicrobial-impregnated central venous catheters. *N. Engl. J. Med.* 1999; 340:1–8. [PubMed: 9878638]
7. Raad I, et al. Central venous catheters coated with minocycline and rifampin for the prevention of catheter-related colonization and bloodstream infections. A randomized, double-blind trial. *Ann. Intern. Med.* 1997; 127:267–274. [PubMed: 9265425]

8. Yorganci K, Krepel C, Weigelt JA, Edmiston CE. Activity of antibacterial impregnated central venous catheters against *Klebsiella pneumoniae*. *Intensive Care Med.* 2002; 28:438–442. [PubMed: 11967598]
9. Jaeger K, et al. Efficacy of a benzalkonium chloride-impregnated central venous catheter to prevent catheter-associated infection in cancer patients. *Chemotherapy.* 2001; 47:50–55. [PubMed: 11125233]
10. Greenfeld JJ, et al. Decreased bacterial adherence and biofilm formation on chlorhexidine and silver sulfadiazine-impregnated central venous catheters implanted in swine. *Crit. Care Med.* 1995; 23:894–900. [PubMed: 7736748]
11. Guay DR. An update on the role of nitrofurans in the management of urinary tract infections. *Drugs.* 2001; 61:353–364. [PubMed: 11293646]
12. Caillier L, et al. Synthesis and antimicrobial properties of polymerizable quaternary ammoniums. *Eur. J. Med. Chem.* 2009; 44:3201–3208. [PubMed: 19380184]
13. Darouiche RO, Mansouri MD, Gawande PV, Madhyastha S. Efficacy of combination of chlorhexidine and protamine sulphate against device-associated pathogens. *J. Antimicrob. Chemother.* 2008; 61:651–657. [PubMed: 18258612]
14. Li P, et al. A polycationic antimicrobial and biocompatible hydrogel with microbe membrane suctioning ability. *Nat. Mater.* 2011; 10:149–156. [PubMed: 21151166]
15. Costa F, Carvalho IF, Montelaro RC, Gomes P, Martins MCL. Covalent immobilization of antimicrobial peptides (AMPs) onto biomaterial surfaces. *Acta Biomater.* 2011; 7:1431–1440. [PubMed: 21056701]
16. Monds RD, O'Toole GA. The developmental model of microbial biofilms: ten years of a paradigm up for review. *Trends Microbiol.* 2009; 17:73–87. [PubMed: 19162483]
17. Holmes PF, et al. Surface-modified nanoparticles as a new, versatile, and mechanically robust nonadhesive coating: suppression of protein adsorption and bacterial adhesion. *J. Biomed. Mater. Res. A.* 2009; 91A:824–833. [PubMed: 19051305]
18. Cheng G, et al. Zwitterionic carboxybetaine polymer surfaces and their resistance to long-term biofilm formation. *Biomaterials.* 2009; 30:5234–5240. [PubMed: 19573908]
19. Cheng G, Zhang Z, Chen SF, Bryers JD, Jiang SY. Inhibition of bacterial adhesion and biofilm formation on zwitterionic surfaces. *Biomaterials.* 2007; 28:4192–4199. [PubMed: 17604099]
20. Hook AL, et al. High-throughput methods applied in biomaterial development and discovery. *Biomaterials.* 2010; 31:187–198. [PubMed: 19815273]
21. Pernagallo S, Wu M, Gallagher MP, Bradley M. Colonising new frontiers-microarrays reveal biofilm modulating polymers. *J. Mater. Chem.* 2011; 21:96–101.
22. Anderson DG, Levenberg S, Langer R. Nanoliter-scale synthesis of arrayed biomaterials and application to human embryonic stem cells. *Nat. Biotechnol.* 2004; 22:863–866. [PubMed: 15195101]
23. Mei Y, et al. Mapping the interactions among biomaterials, adsorbed proteins, and human embryonic stem cells. *Adv. Mater.* 2009; 21:2781–2786.
24. Mei Y, et al. Combinatorial development of biomaterials for clonal growth of human pluripotent stem cells. *Nat. Mater.* 2010; 9:768–778. [PubMed: 20729850]
25. Yang J, et al. Polymer surface functionalities that control human embryoid body cell adhesion revealed by high-throughput surface characterization of combinatorial material microarrays. *Biomaterials.* 2010; 31:8827–8838. [PubMed: 20832108]
26. Berger H, Hacker J, Juarez A, Hughes C, Goebel W. Cloning of the chromosomal determinants encoding hemolysin production and mannose-resistant hemagglutination in *Escherichia coli*. *J. Bacteriol.* 1982; 152:1241–1247. [PubMed: 6754701]
27. Hidron AI, et al. Antimicrobial-resistant pathogens associated with healthcare-associated infections: annual summary of data reported to the national healthcare safety network at the Centers for Disease Control and Prevention, 2006–2007. *Infect. Control Hosp. Epidemiol.* 2008; 29:996–1011. [PubMed: 18947320]
28. Schumm K, Lam TB. Types of urethral catheters for management of short-term voiding problems in hospitalised adults. *Cochrane DB. Syst. Rev.* 2008; 16:CD004013.

29. Katsikogianni M, Missirlis YF. Concise review of mechanisms of bacterial adhesion to biomaterials and of techniques used in estimating bacteria-material interactions. *Eur. Cell. Mater.* 2004; 8:37–57. [PubMed: 15593018]
30. O'Toole G, Kaplan HB, Kolter R. Biofilm formation as microbial development. *Annu. Rev. Microbiol.* 2000; 54:49–79. [PubMed: 11018124]
31. Flemming HC, Wingender J. The biofilm matrix. *Nat. Rev. Microbiol.* 2010; 8:623–633. [PubMed: 20676145]
32. Urquhart AJ, et al. High-throughput surface characterisation of a combinatorial material library. *Adv. Mater. (Deerfield Beach Fla.)*. 2007; 19:2486–2491.
33. Davies MC, et al. High-throughput surface characterization: a review of a new tool for screening prospective biomedical material arrays. *J. Drug Target.* 2010; 18:741–751. [PubMed: 20945971]
34. Hook AL, et al. Polymers with hydro-responsive topography identified using high-throughput AFM of an acrylate microarray. *Soft Matter.* 2011; 7:7194–7197. [PubMed: 23259005]
35. Taylor M, et al. Partial least squares regression as a powerful tool for investigating large combinatorial polymer libraries. *Surf. Interface Anal.* 2009; 41:127–135.
36. Urquhart AJ, et al. TOF-SIMS analysis of a 576 micropatterned copolymer array to reveal surface moieties that control wettability. *Anal. Chem.* 2008; 80:135–142. [PubMed: 18044847]
37. Dalton, HM.; March, PE. Molecular genetics of bacterial adhesion and biofouling. In: An, YH.; Friedman, RJ., editors. *Handbook of Bacterial Adhesion: Principles, Methods, and Applications*. Humana Press; 2000. p. 43-51.
38. Ong YL, Razatos A, Georgiou G, Sharma MM. Adhesion forces between *E. coli* bacteria and biomaterial surfaces. *Langmuir.* 1999; 15:2719–2725.
39. Conrad JCCJC, et al. Flagella and pili-mediated near-surface single-cell motility mechanisms in *P. aeruginosa*. *Biophys. J.* 2011; 100:1608–1616. [PubMed: 21463573]
40. Williams P, Winzer K, Chan WC, Camara M. Look who's talking: communication and quorum sensing in the bacterial world. *Philos. Trans. R. Soc. Lond. B. Biol. Sci.* 2007; 362:1119–1134. [PubMed: 17360280]
41. Ferrieres L, Clarke DJ. The RcsC sensor kinase is required for normal biofilm formation in *Escherichia coli* K-12 and controls the expression of a regulon in response to growth on a solid surface. *Mol. Microbiol.* 2003; 50:1665–1682. [PubMed: 14651646]
42. Gilbert KB, Kim TH, Gupta R, Greenberg EP, Schuster M. Global position analysis of the *Pseudomonas aeruginosa* quorum-sensing transcription factor LasR. *Mol. Microbiol.* 2009; 73:1072–1085. [PubMed: 19682264]
43. Harder P, Grunze M, Dahint R, Whitesides GM, Laibinis PE. Molecular conformation in oligo(ethylene glycol)-terminated self-assembled monolayers on gold and silver surfaces determines their ability to resist protein adsorption. *J. Phys. Chem. B.* 1998; 102:426–436.
44. Taylor M, Urquhart AJ, Zelzer M, Davies MC, Alexander MR. Picoliter water contact angle measurement on polymers. *Langmuir.* 2007; 23:6875–6878. [PubMed: 17503858]
45. Messina, M. PhD thesis. Univ. Nottingham; 2010. Gene Regulation in *Pseudomonas Aeruginosa*: from Environmental Signals to Responses via Global Post-Transcriptional Control and Intracellular Messaging.
46. Qazi SNA, Rees CED, Mellits KH, Hill PJ. Development of GFP vectors for expression in *Listeria monocytogenes* and other low G+C gram positive bacteria. *Microb. Ecol.* 2001; 41:301–309. [PubMed: 12032603]
47. Brooks T, Keevil CW. A simple artificial urine for the growth of urinary pathogens. *Lett. Appl. Microbiol.* 1997; 24:203–206. [PubMed: 9080700]
48. Diggle SP, et al. The galactophilic lectin, LecA, contributes to biofilm development in *Pseudomonas aeruginosa*. *Environ. Microbiol.* 2006; 8:1095–1104. [PubMed: 16689730]
49. Johansson EMV, et al. Inhibition and dispersion of *Pseudomonas aeruginosa* biofilms by glycopeptide dendrimers targeting the fucose-specific lectin LecB. *Chem. Biol.* 2008; 15:1249–1257. [PubMed: 19101469]
50. Kuklin NA, et al. Real-time monitoring of bacterial infection in vivo: Development of bioluminescent staphylococcal foreign-body and deep-thigh-wound mouse infection models. *Antimicrob. Agents Chemother.* 2003; 47:2740–2748. [PubMed: 12936968]

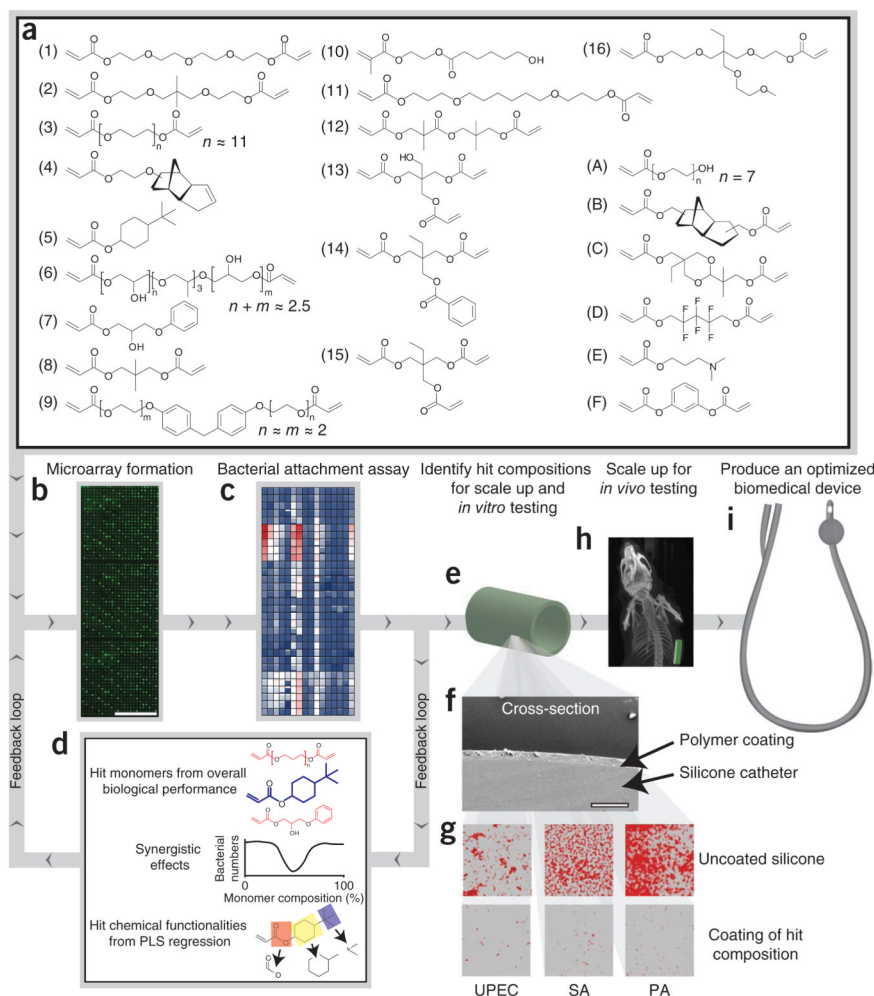
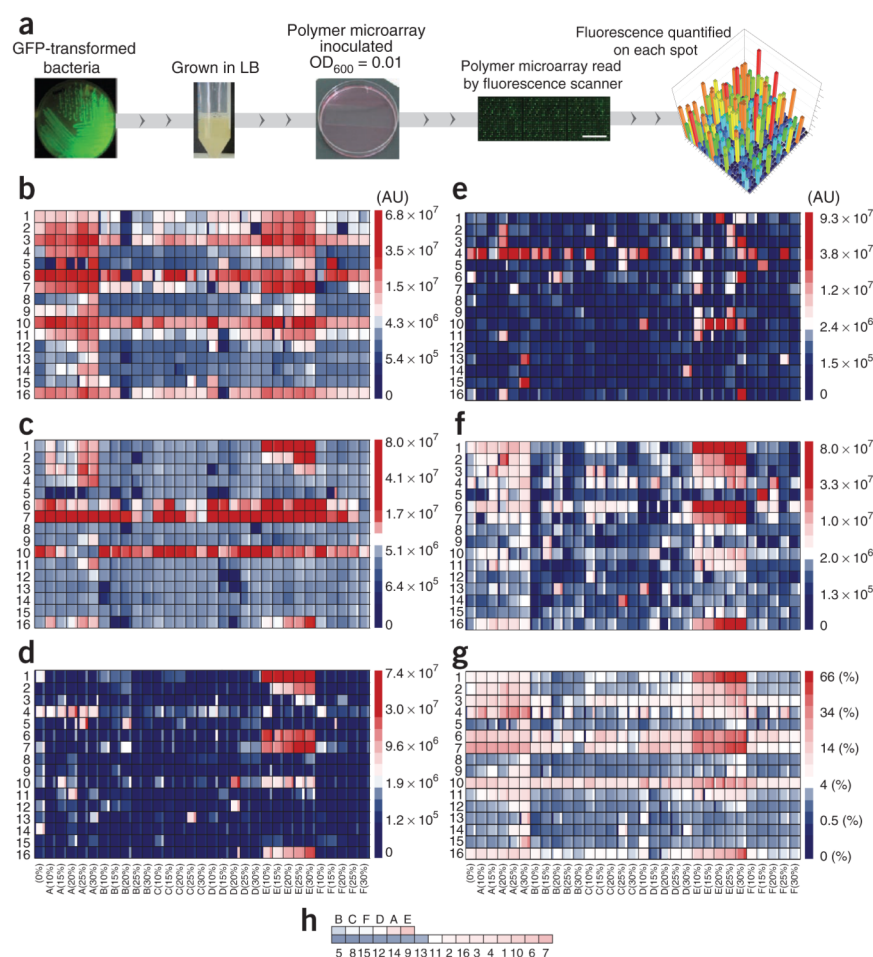
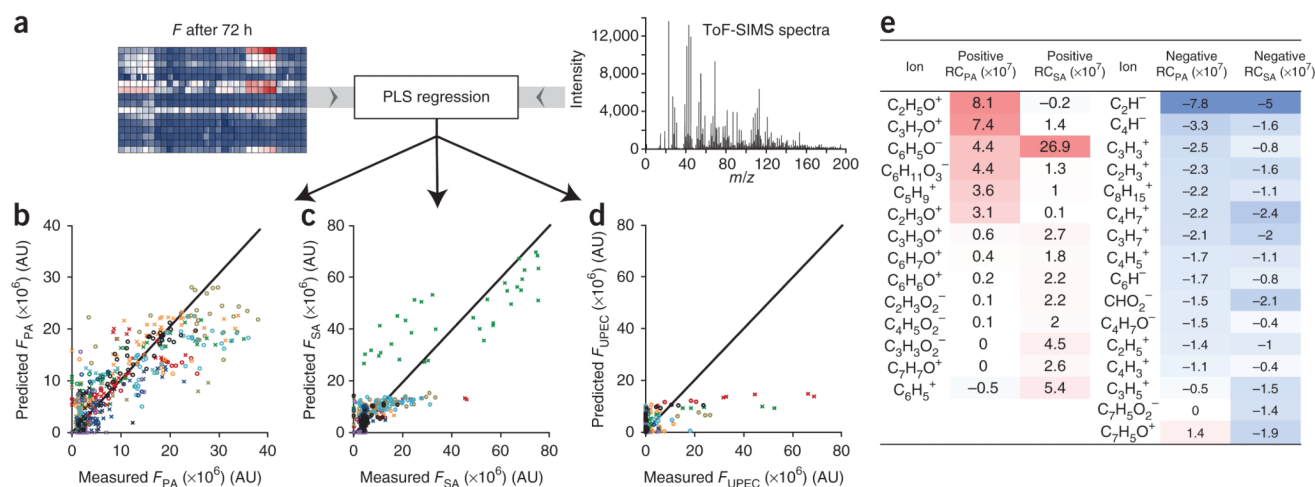


Figure 1. Schematic of the approach used to identify hit materials resistant to bacterial attachment and scale-up of hit materials. **(a)** The chemical structures of the monomers. **(b–f)** Outline of the strategy utilized for identifying hit material composition. **(b)** Fluorescence scanning image of the first-generation microarray after incubation with *P. aeruginosa* for 72 h. Three replicate arrays were present on each glass slide. Scale bar, 10 mm. **(c)** Intensity map of the bacterial data from the first-generation array. **(d)** The feedback loop used to select monomer compositions for a second-generation array. The biological performance of each monomer, the identification of hit material compositions that have synergistic effects and the results from the PLS regression of ToF-SIMS spectra and bacterial data were used to inform the composition of the second-generation array. **(e)** Schematic representation of the hit material composition scaled up. **(f)** An SEM image of the cross-section of a silicone catheter coated with a hit polymer (thickness, 20–25 μm). Scale bar, 100 μm . **(g)** Confocal images of SYTO17-stained biofilm for the three pathogens studied (*P. aeruginosa* (PA), *S. aureus* (SA), UPEC) from coated and uncoated silicone catheters. Each image is 160 \times 160 μm . **(h)** Microcomputed tomography scan of a coated catheter implanted subcutaneously into a murine model. The catheter has been colored green in this image. **(i)** A schematic representation of a catheter coated with the hit composition.

**Figure 2.**

Slide inoculation procedure and ‘heatmaps’ of bacterial fluorescent intensity determined from first-generation slides (**a**) Bacterial attachment assay procedure. (**b–f**) Intensity maps of *F* measured for each bacterial strain on the first-generation array after 72-h incubation; *P. aeruginosa* (**b**), *S. aureus* (**c**), UPEC (**d**), UPEC grown in artificial urine (**e**) and UPEC grown on an artificial urine-conditioned slide (**f**). (**g**) Intensity map of the λ obtained for each material in the array, given as a percentage of the maximum bacterial numbers for all strains at all culture conditions. The major monomers are listed on the y-axis whereas the composition of the minor monomers is shown on the x-axis. The large shaded area within each outlined area indicates the mean value, and the mean \pm 1 s.d. unit is presented in the narrow columns to the right (plus) and left (minus) of the mean, $n = 3$. Key to right. A square-root scale is applied to the intensity indicators. (**h**) The average λ for all materials containing a specific monomer, ranked from lowest to highest. The major and minor monomers were considered separately. The color next to each monomer is indicative of that monomer’s mean λ and is colored by the same intensity scale as in **g**.

**Figure 3.**

Correlation of the surface chemistries represented in the ToF-SIMS. **(a)** Schematic depiction of the PLS regression model used to predict the biological performance of materials by correlating F with the ToF-SIMS spectra. **(b–d)** The predicted bacterial attachment determined from the PLS regression model for *P. aeruginosa* (PA) ($R^2 = 0.68$) **(b)**, *S. aureus* (SA) ($R^2 = 0.76$) **(c)**, and UPEC ($R^2 = 0.28$) **(d)**. The $y = x$ line is drawn as a guide. Polymers are grouped according to the major monomer 1 (×), 2 (○), 3 (×), 4 (○), 5 (×), 6 (○), 7 (×), 8 (○), 9 (×), 10 (○), 11 (×), 12 (○), 13 (×), 14 (○), 15 (×), 16 (○). **(e)** The key ions identified to be important by ToF-SIMS PLS regression analysis for the surface attachment of both *P. aeruginosa* (PA) and *S. aureus* (SA). The regression coefficient (RC) for each ion is also shown from the regression analysis with each bacterium separately. The RCs have been shaded according to their value (red, positive; blue, negative; white, neutral).

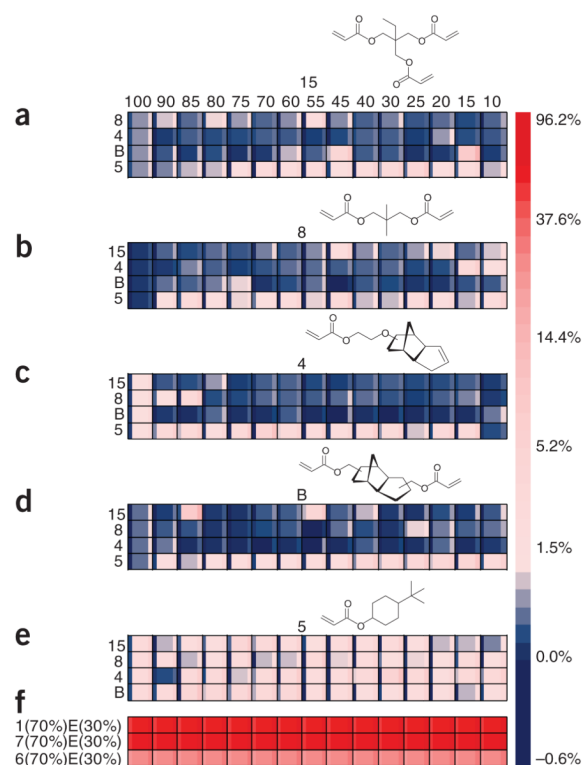


Figure 4.

λ determined for all materials represented in the second-generation array. Five monomers from the first-generation array were mixed pairwise at 14 different ratios (15, 5, 8 and B were mixed with each other and monomer 4 at ratios of $x:(1-x)$ where x varied from 10 to 90). The content of the major monomer is indicated along the x -axis: (a) 15, (b) 8, (c) 4, (d) B and (e) 5 (Fig. 1a). The co-monomer is indicated in the y -axis. (f) The λ determined for high-bacterial-attachment polymers included in the second-generation array from the first-generation array. A square-root scale is applied to the color bar to highlight the low λ measured for this array. The mean of each value is shown as the large shaded area within each outlined rectangle and the mean ± 1 s.d. unit is presented in the narrow columns to the right (plus) and left (minus) of the mean, $n = 4$.

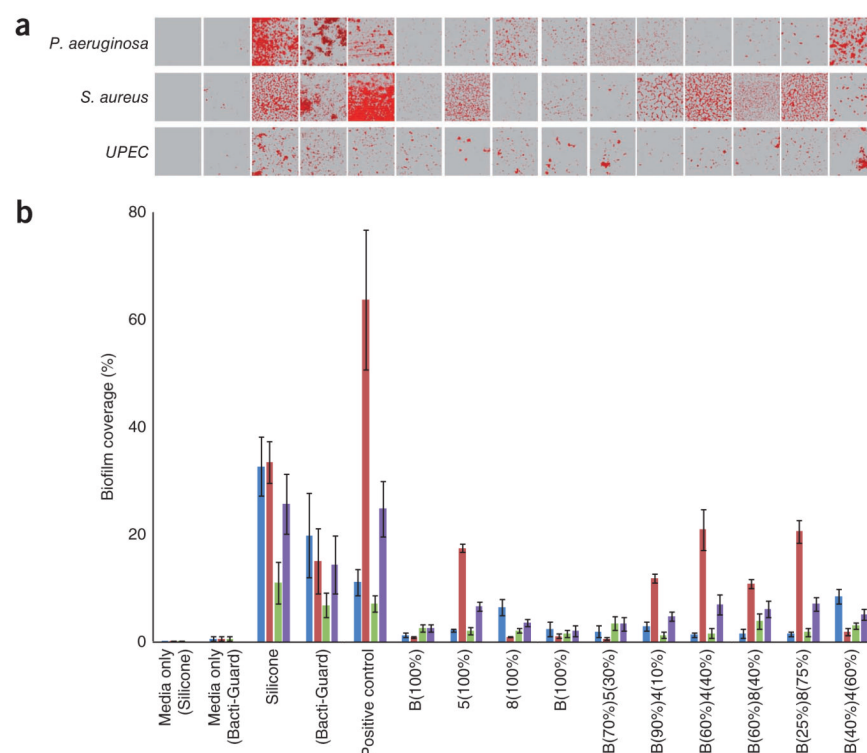


Figure 5.

Proportion of surface covered by bacteria on catheters coated with hit polymers after 72 h incubation with planktonic bacteria. **(a)** Confocal microscopy images of *P. aeruginosa*, *S. aureus* and UPEC stained with SYTO17 growing on coated catheters, uncoated silicone and silicone treated with media without bacteria as a controls. Each image is $160 \times 160 \mu\text{m}$. **(b)** Quantification of bacterial area coverage for *P. aeruginosa* (blue), *S. aureus* (red), UPEC (green) and \downarrow (purple) from confocal images of each sample. Area coverage was normalized to the coverage on silicone. The error bars represent mean \pm 1 s.d. unit, $n = 5$. The composition of the positive control was specific to the bacterial strain used: *P. aeruginosa* = 6(100%), *S. aureus* = 7(100%), UPEC = 1(70%)E(30%). The fluorescence signal observed on the media-only controls is due to auto-fluorescence of the substrate and translates to a small erroneous ($<0.5\%$) estimate of area of surface covered with bacteria.

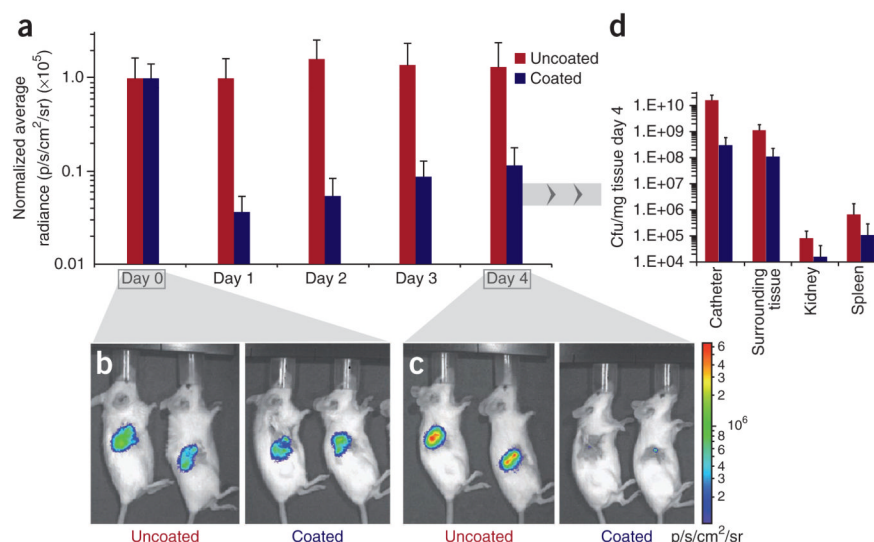


Figure 6.

In vivo performance of hit polymer. Catheters dip-coated with hit polymer 4 copolymerized with DEGMA were implanted subcutaneously in mice. Mice were inoculated after 1 d with *S. aureus* *Xen29*, which were injected into the center of the tube. (a) The bioluminescence at the infection site was measured on the day of inoculation (day 0) and for the next 4 d. Error bars, ± 1 s.d. unit; $n = 9$ (three separate experiments, each comprising three control catheter mice and three polymer-coated catheter mice). The difference in bioluminescence between coated and uncoated samples from day 1 to 4 was confirmed to 99.5% confidence (*t*-test). Bioluminescence was normalized to the output at day 0 and all measurements have had the background luminescence subtracted, measured from an implanted catheter prior to inoculation. (b,c) Luminescence images with overlaid brightfield images of mice implanted with both uncoated (left) and coated (right) catheter segments on day 0 (b) and day 4 (c). (d) At day 4 the mice were euthanized, the insertion site plus the kidneys and spleen harvested, and the number of bacteria on the tissue determined. Error bars, ± 1 s.d. unit; $n = 3$ (taken from one group of three). The difference in cfu counts between coated and uncoated samples was confirmed to 99% confidence for the catheter and surrounding tissue, to 90% confidence for the kidneys and to 75% confidence for the spleen (*t*-test).